Seismic Fragility Analysis of Reinforced Concrete Bridges with Chloride Induced Corrosion Subjected to Spatially Varying Ground Motions

Chao Li[1, 2, *], Hong Hao[2], Hongnan Li[1] and Kaiming Bi[2]

[1]Institute of Earthquake Engineering, Faculty of Infrastructure Engineering, Dalian University of Technology, Dalian 116024, China
[2]Department of Civil Engineering, Curtin University, Kent Street, Bentley WA 6102, Australia

Abstract: This paper studies the time-dependent seismic fragility of reinforced concrete bridges with chloride induced corrosion under spatially varying ground motions. The time-varying characteristic of the chloride corrosion current density and the uncertainties related to the structural, material and corrosion parameters are both considered in the probabilistic finite element modelling of the example RC bridge at different time steps during its life-cycle. Spatially varying ground motions at different bridge supports are stochastically simulated and used as inputs in the fragility analysis. Seismic fragility curves of the corroded RC bridge at different time steps are generated using the probabilistic seismic demand analysis method. Numerical results indicate that both chloride induced corrosion and ground motion spatial variations have a significant effect on the bridge structural seismic fragility. As compared to the intact bridge, the mean PGAs of the fragility curves of the example RC bridge are decreased by approximately 40% after 90 years since corrosion initiation. Moreover, the effect of ground motion spatial variations changes along with the process of chloride induced corrosion owing to the structural stiffness degradation. Neglecting seismic ground motion spatial variations might not lead to an accurate estimation of the lifetime seismic fragility of RC bridges with chloride induced corrosion.

Key words: reinforced concrete bridges, life-cycle, seismic fragility, chloride induced corrosion, spatially varying ground motions

1. Introduction

Bridges are important lifeline structures and their damage during earthquake actions can cause significant economic loss and hamper the post-earthquake relief efforts. Seismic fragility analysis method[1-4], which can provide the structural damage probability under a certain level of earthquake ground motion intensity, is a powerful tool for the seismic risk assessment of bridge structures. The seismic fragility analysis method can be conducted through either an empirical or analytical way. Empirical fragility curves[5-6] are generated based on the bridge damage data observed from past earthquakes. However, the application of empirical fragility curves is greatly constrained by the insufficiency of bridge damage data in actual earthquakes and the possible inapplicability for the bridges located in areas other than the original earthquake region. Analytical fragility curves[7-10] are developed through bridge structural finite element modelling and the corresponding seismic response analysis, in which the uncertainties related to structural modelling and input seismic ground motions can be reasonably considered. The analytical fragility curves can be in good agreement with the empirical ones.[6] Therefore it is widely used both in the field of academic research and engineering practice.

*Corresponding author. E-mail: lichao17007@163.com

Recently, reports from the American Society of Civil Engineers[11] indicated that more than 20% of the 607,380 bridges in the USA need significant repair or replacement to ensure their normal service functions and anti-seismic capacities. Bridge structure conditions inevitably deteriorate during its service owing to many factors. Among them corrosion is one of the critical sources that cause structural performance degradations. Neglecting the environmental corrosion effects may lead to significant underestimation of the structural seismic fragility along the service life of a bridge. Chloride induced corrosion is one of the most serious corrosion effects for the reinforced concrete bridges located in coastal areas or in regions where deicing salts are heavily used.[12-13] Many researchers have considered the corrosion-induced structural condition deterioration in their studies of the seismic fragility of RC bridges during their life-cycles. Choe *et al.*[14] estimated the seismic fragility of a RC bridge with chloride induced corrosion through a probabilistic capacity reduction model of corroded RC columns. Simon *et al.*[15] investigated the effect of corrosion induced reinforcement sectional area reduction and concrete cover spalling on the seismic fragility of RC bridges. By taking into account the degradation of column reinforcement diameter and yield strength induced by chloride corrosion, Alipour *et al.*[16] performed seismic fragility analysis of RC bridge structures. Nevertheless, the random fluctuations of the structural and corrosion parameters, which are inevitable and may have a significant impact on the bridge structural seismic fragility, were not considered in their studies. Ghosh and Padgett[17] carried out a system level time-dependent seismic fragility analysis by considering the combined influences of RC column and steel bearing corrosions. All these studies indicate that the seismic fragility of RC bridges increase during their life-cycles owing to the chloride induced corrosion.

To have a better understanding of the seismic fragility increasing trend of a RC bridge along its service life, reasonably modelling the process of chloride induced corrosion is very important. Many research results[18-19] indicate that the corrosion rate of reinforcing bars in the RC components exposed to the attack of chloride ions is reduced with time. However, in most seismic fragility analyses reported in the literature, the corrosion rate is assumed to be a constant during the corrosion process, which might lead to an unreasonable estimation of the lifetime seismic fragility of corroded RC bridges. In this paper, the reinforcement corrosion degree based on an empirical time-varying corrosion current density model[20] is formulated, and the uncertainties related to structural, material and corrosion process are considered to study the lifetime seismic fragility of corroded RC bridges.

In all the aforementioned seismic fragility analyses, the seismic responses of bridge structures are calculated using uniform ground excitations and the spatial variations of seismic ground motions are neglected. The main factors that may lead to spatial variations in seismic ground motions include: the wave passage effect due to the different arrival times of earthquake waves at different structural supports; the coherency loss caused by multiple scatterings of waves in the soil medium; and the local site effect owing to the difference in local soil conditions. In fact, many previous studies[21-24] have shown that the ground motion spatial variations have a significant effect on the seismic response of long span structures such as bridges. Therefore, it is essential to consider the spatial variability of the input ground motions in the bridge seismic fragility analysis. The studies related to the seismic fragility analysis of bridge structures subjected to spatial ground motions are very limited. Deodatis *et al.*[25] developed the seismic fragility curves accounting for the ground motion spatial variations for the first time; Kim *et al.*[26] compared the bridge seismic fragility under uniform and spatially varying ground motions; Lupoi *et al.*[27] conducted the seismic fragility analysis for RC bridges with spatial ground motions including the local site effect. However, the possible bridge condition deterioration owing to chloride induced corrosion was not considered in these seismic fragility analyses.

To achieve a more realistic seismic fragility estimation of the RC bridges during their life-cycles, both of the time-varying characteristic of the chloride corrosion current density and the ground motion spatial variations are considered in the seismic fragility analysis in this study. The analysing steps are as follows: Firstly, the finite element models of the example RC bridge at different time steps during its life-cycle are built by considering the chloride induced corrosion effect and the parameter uncertainties. Secondly, the three-dimensional spatial ground motions are stochastically simulated by considering wave passage effect, coherency loss effect and local site effect. Finally, seismic fragility curves of the corroded RC bridges subjected to the simulated spatial ground motions are generated based on the probabilistic seismic demand analysis method and the influences of ground motion spatial variations on the lifetime seismic fragility of the corroded RC bridges are investigated in detail. It should be noted that soil-structure interaction (SSI) can further alter the seismic responses of bridge structures[23, 28], however, the primary objective of the present study is to investigate the influence of ground motion spatial variations on the lifetime seismic fragility of RC bridge structures with chloride induced corrosion, not to further complicate this problem, SSI is not considered in the present study.

2. Bridge Modelling under Chloride Induced Corrosion

2.1. Bridge description

A three-span continuous rigid frame reinforced concrete bridge located in an offshore environment is employed as an example in the present study. The bridge is designed according to the Chinese seismic design code[29] and the effect of chloride induced corrosion is not considered in the structural seismic design. The elevation view and the cross sections of the bridge are shown in Fig. 1. The superstructure is a pre-stressed concrete double-cell box girder with a uniform cross section and the piers are reinforced concrete single columns with a circular section. The standard compressive strengths of the concrete are 29.6 MPa and 32.4 MPa for the columns and superstructure, respectively. The yield strength of the reinforcing bars is 400 MPa. A 50 mm gap is introduced at end of the superstructure to accommodate the temperature induced shrinkage. The piers and abutments are supported on pile foundations. Since the piers are the most vulnerable elements during earthquake actions, the chloride induced corrosion is only considered for the columns, the corrosion of the superstructure and the abutments are neglected.

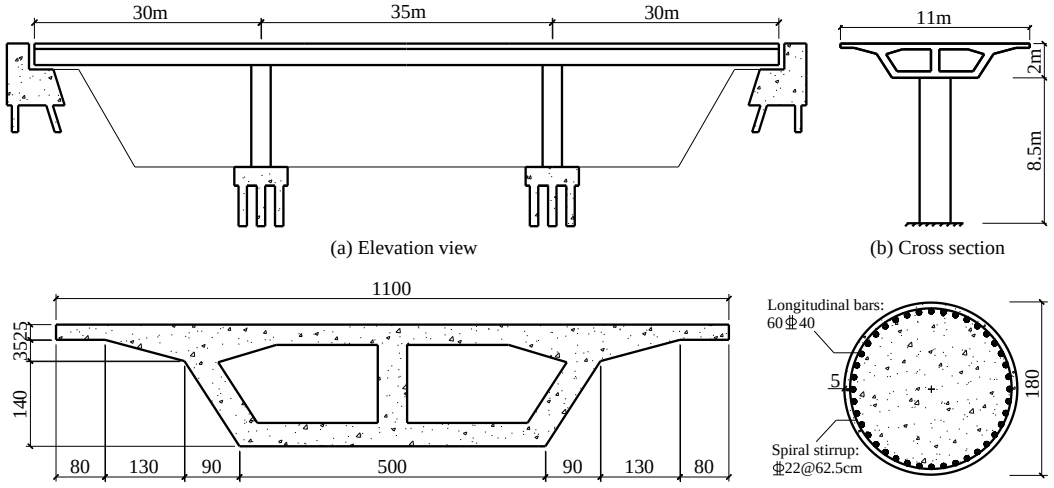

(a) Elevation view (b) Cross section

(c) Superstructure section (mm) (d) Pier section (mm)

Fig. 1. Elevation view and the cross sections of the example bridge

To consider the influence of local site conditions, both homogeneous and heterogeneous site conditions are assumed in this study. Fig. 2 shows the schematic view of the site

conditions, where Points 1 and 4 represent abutment supports and Points 2 and 3 represent pier column supports. Either firm site (Class I in the Chinese design code) or medium site (Class II) is assumed for all the supports in the homogeneous site case. In the heterogeneous site case, medium site is assumed at the abutment supports while firm site for the column supports.

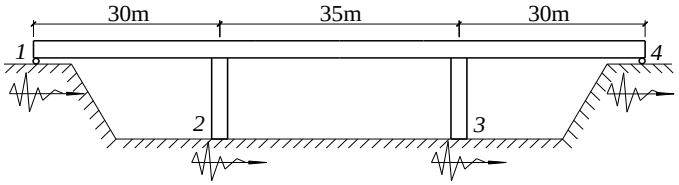

Fig. 2. Schematic view of the site condition of the bridge structure

2.2. Chloride induced corrosion effect

In a coastal zone, the water-borne chloride ions are accumulated on the surface of the RC bridges under the transportation of sea winds. The diffusion of chloride ions is induced by the chloride concentration difference between the surface and interior part of the concrete. As the primary reason of transportation of the chloride ions, the diffusion process can be represented by the Fick's second law[13]

$$\frac{\partial C(x,t)}{\partial t} = -D_c \frac{\partial^2 C(x,t)}{\partial x^2} \tag{1}$$

where $C(x, t)$ is the chloride concentration in the depth of x from the surface of the concrete cover at t years and D_c is the coefficient of diffusion. McGee[30] suggested that the chloride concentration on the concrete cover surface is constant with time for the offshore RC structures. In this case, the corrosion initiation time of reinforcements in RC components can be expressed as

$$T_i = \frac{d_c^{\,2}}{4D_c}\left[\text{erf}^{-1}\left(\frac{C_s - C_{cr}}{C_s}\right)\right]^{-2} \tag{2}$$

in which d_c is the depth of the concrete cover; C_s represents the chloride concentration on the cover surface and C_{cr} denotes the critical chloride concentration corresponding to the corrosion initiation time. Table 1 lists the probability distributions of the parameters in Eq. (2) for the example bridge columns by referencing the corrosion properties of RC components in coastal environments[30-31]. Monte Carlo simulation method is adopted to calculate the corrosion initiation time of the column reinforcements. As shown in Fig. 3, the mean value and standard deviation are virtually unchanged when the sample size reaches 50000, indicating that the simulation is converged. A lognormal distribution with a mean of 15.4 years and a standard deviation of 8.7 years can be a good fit for the corrosion initiation time of the reinforcements. Fig. 4 shows the comparison between the Monte Carlo simulation results and the probability density function curve of the lognormal distribution.

Table 1. Probability distribution models of the parameters related to the reinforcement corrosion initiation time, adopted from [30-31]

Parameter	Unit	Distribution	Mean	COV
d_c	mm	Lognormal	50	0.1
C_s	kg/m^3	Lognormal	2.95	0.49
C_{cr}	kg/m^3	Uniform(0.6-1.2)	0.9	0.19
D_c	cm^2/s	Lognormal	3×10^{-8}	0.3

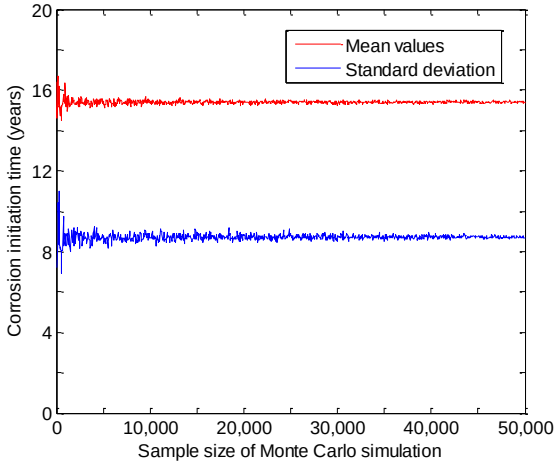

Fig. 3. Converge test of the reinforcement corrosion initiation time

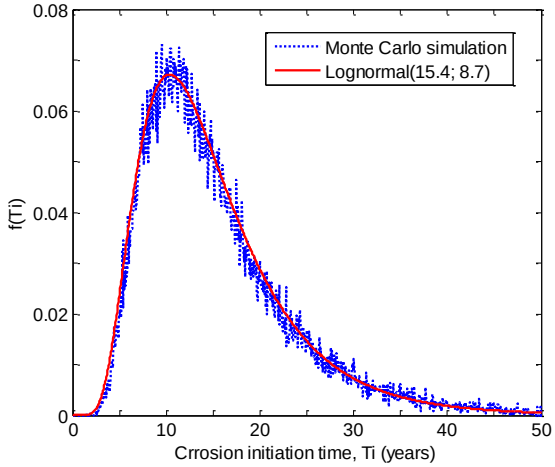

Fig. 4. Comparison of Monte Carlo simulation result and lognormal distribution

In the reinforcement corrosion stage, the water-insoluble iron hydroxide produced by corrosion will attach to the reinforcement surface and decrease the corrosion rate. Vu and Stewart[20] developed an empirical equation for the time-dependent reinforcement corrosion current density for the RC components under chloride induced corrosion, namely

$$i_{corr}(t_i) = 0.85 i_{corr,0} t_i^{-0.29} \tag{3}$$

$$i_{corr,0} = \frac{37.8(1-w/c)^{-1.64}}{d_c} (\mu \mathrm{A}/\mathrm{cm}^2) \tag{4}$$

in which t_i represents the time after corrosion initiation; $i_{corr,0}$ is the corrosion current density at the corrosion initiation time, w/c denotes the water to cement ratio and d_c is the concrete cover depth.

The diameters and mechanical properties of the reinforcements deteriorate with the proceeding of the chloride induced corrosion. Based on experimental results, Du *et al.*[32] proposed the time-dependent diameter and yield strength model for the reinforcements in RC components under chloride induced corrosion:

$$d_s(t_i) = \sqrt{1-Q_{corr}(t_i)} \cdot d_{s0} \tag{5}$$

$$f_y(t_i) = (1.0 - \beta_y Q_{corr}(t_i)) f_{y0} \tag{6}$$

where $d_s(t_i)$ and $f_y(t_i)$ are the reinforcement diameter and yield strength at time after corrosion initiation, respectively; d_{s0} and f_{y0} are the initial reinforcement diameter and yield strength, respectively; β_y is the strength reduction factor, the value of β_y ranges from 0.16 to 0.45 for ribbed bars as suggested in previous studies[32, 33] and a reasonable compromise value of 0.3 is adopted in this study; $Q_{corr}(t_i)$ is the percentage of the corroded mass relative to the initial mass of the reinforcement, which can be formulated as

$$Q_{corr}(t_i) = \frac{4x_{corr}(t_i)}{d_{s0}} \left(1 - \frac{x_{corr}(t_i)}{d_{s0}}\right) \tag{7}$$

where x_{corr} is the corroded depth of the reinforcement. When the corrosion current density is taken as a constant, x_{corr} can be expressed as

$$x_{corr} = 0.0116 i_{corr} t_i \tag{8}$$

In this study, the time-dependent property of corrosion current density is considered. The empirical model in Eq. (3) is substituted into Eq. (8) and then conducting integration in the time domain. The time-dependent percentage of the corroded mass relative to the initial mass of the reinforcement is reformulated as

$$Q_{corr}(t_i) = \frac{2.10(1-w/c)^{-1.64}}{d_c d_{s0}} t_i^{0.71} - \frac{1.10(1-w/c)^{-3.28}}{d_c^2 d_{s0}^2} t_i^{1.42} \quad (9)$$

Combining Eq. (9) with Eqs. (5) and (6), the reinforcement diameter and yield strength at different time steps based on the time-dependent corrosion current density can be calculated. It should be noted that since the large uncertainty of the reinforcement corrosion initiation time (COV=0.563) will cause a larger variation in the calculation of $Q_{corr}(t_i)$, the time after corrosion initiation is used to calculate the time-dependent reinforcement diameter and yield strength in this study. In other words, the results presented in this study do not start from the time when the bridge begin its service, but from the time when reinforcement bar corrosion starts. If it is of more interests to account for the bridge conditions from the time it is in service, the corrosion initiation time should be included.

Monte Carlo simulation method is used to again calculate the probabilistic distributions of the column reinforcement diameter and yield strength at a time interval of 15 years based on Eqs. (5), (6) and (9). The uncertainties of the relevant parameters[12, 34-35] are listed in Table 2. The simulation results show that the corresponding values are all converged using a sample size of 50000, and can be represented by lognormal distributions. Fig. 5 shows the time-dependent mean values and probability distribution functions (PDFs) of the reinforcement diameter and yield strength. It can be concluded that the mean values of these two parameters decrease with time while the coefficients of variation increase with time. The increasing trend of the coefficient of variation of yield strength is not obvious due to the reduction effect of the strength reduction factor β_y. It can be also noticed that the degradation degrees of both these two parameters present a decreasing tendency due to the decreasing of the chloride corrosion current density.

Table 2. Probabilistic distributions of parameters relevant to $d_s(t_i)$ and $f_y(t_i)$

Parameters	Units	Distribution	Distribution parameters
w/c	-	Triangular	Mean=0.5, Min=0.45, Max=0.55
d_c	mm	Lognormal	Mean=50, COV=0.1
d_{s0}	mm	Lognormal	Mean=40, COV=0.02
f_{y0}	MPa	Lognormal	Mean=400, COV=0.08

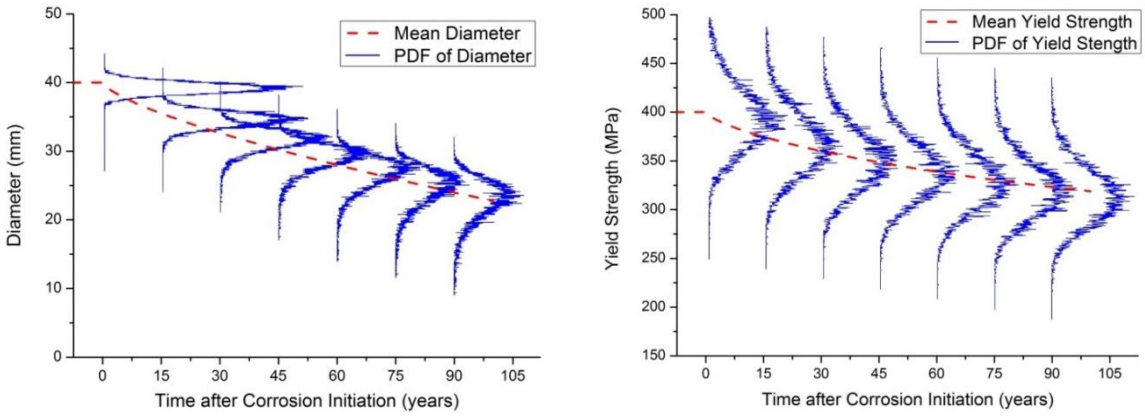

(a) Diameter (b) Yield strength

Fig. 5. Mean values and probability distributions of the reinforcement diameter and yield strength

It should be noted that the effect of the concrete cover cracking or spalling on the fragility of the RC bridge is neglected in the present study, since previous study by Simon *et al.*[15] has shown that the effect of the concrete cover spalling on the seismic fragility of RC bridges is very limited. Furthermore, it is reasonable to neglect the loss of bond-slip strength induced by corrosion for the well confined column designed according to the code, as demonstrated by Fang *et al.*[36].

2.3. Bridge numerical modelling

The OpenSees analysis platform[37] is used to model the example RC bridge. In seismic design of bridge structures, the superstructure is required to remain in linear elastic range while the columns are permitted to enter the nonlinear range. Therefore, the superstructure is modelled with elastic beam-column elements which are subjected to uniform dead loads represented by weight per unit length of the deck. The columns are modelled using nonlinear beam-column elements whose cross section is defined with a number of fibres including confined concrete, longitudinal reinforcements and cover concrete, which are represented by Material Concrete04, Steel02 and Concrete01, respectively. Since the example bridge is a continuous rigid frame, rigid links are used to connect the superstructure and the pier columns. The abutment is modelled by referencing previous works[16, 38], a rigid element with a length of the superstructure width is employed and a rigid connection is placed between the superstructure centreline and the rigid element. The rigid element is supported by an elastic spring in the vertical direction and nonlinear zero-length elements with a passive stiffness k_a in the two horizontal directions at the two ends. In addition, a gap element allowing only longitudinal translation is defined to model the gap between the superstructure and the abutments.

In this study, the uncertainties in structural, material and chloride induced corrosion related parameters are considered, i.e., the column concrete compressive strength (f_c), the mass per unit length of the deck (m_d), the abutment stiffness (k_a), the expansion gap width (w_g)[9, 35] and the above obtained time-dependent column reinforcement diameter ($d_s(t_i)$) and yield strength ($f_y(t_i)$). Latin hypercube sampling method is applied to build 10 3D bridge finite element models at every 15-year time step after the column reinforcement corrosion initiation time.

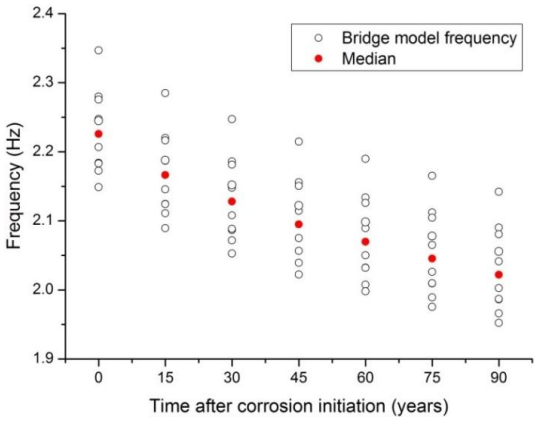

Fig. 6. Time-dependent fundamental frequencies of the bridge models

The fundamental frequencies of the 10 bridge models at each time step during the bridge's life-cycle are calculated, as plotted in Fig. 6. The median of the 10 frequencies at each time step is also calculated, it can be seen that the median of the basic frequencies of the corroded bridges at initial and 90 years after corrosion initiation are 2.226 and 2.022 Hz respectively with a decreasing of 9.2%. Moreover, the degradation trend of the fundamental frequency decreases with time due to the reduction of corrosion rate in the bridge's life-cycle.

3. Spatially Varying Ground Motions

The three-dimensional spatially varying ground motions are stochastically simulated based on the method proposed by Bi and Hao[39]. This method can be used to conveniently consider the influence of local soil conditions. In the present study, the ground motion time histories at different supports of the example bridge are compatible with the response spectra defined in the Chinese design code[29]. Two site conditions are considered, namely Class I (firm site) and Class II (medium site) as stated in the code. The response spectra for the two site conditions are shown in Fig. 8. The spatial variation of ground motions at four supports of the example

bridge is modelled by an empirical coherency loss function proposed by Hao *et al.*[40] based on the recorded strong ground motions during Event 45 at the SMART-1 array. The coherency loss between ground motions at location *i* and *j* is expressed as

$$\gamma_{ij}(i\omega, d_{ij}) = \exp(-\beta d_{ij}) \exp\left[-\alpha(\omega)\sqrt{d_{ij}}(\omega/2\pi)^2\right] \exp(i\omega d_{ij}/v_{app}) \tag{10}$$

where

$$\alpha(\omega) = \begin{cases} 2\pi a/\omega + b\omega/2\pi + c, & 0.314\,rad/s \le \omega \le 62.83\,rad/s \\ 0.1a + 10b + c, & \omega > 62.83\,rad/s \end{cases} \tag{11}$$

in which d_{ij} is the distance between location *i* and *j*; *a*, *b*, *c* and β are constants obtained from regression analysis of the ground motions during Event 45, these parameters represent highly correlated ground motions. In this study, two more groups of modified parameters which represent intermediately and weakly correlated ground motions are used for comparison purpose, the corresponding parameters are listed in Table 3.

Table 3. Parameters for coherency loss functions

Coherency	β ($\times 10^{-4}$)	a ($\times 10^{-3}$)	b ($\times 10^{-5}$)	c ($\times 10^{-4}$)
Highly(Event 45)	1.109	3.583	-1.811	1.177
Intermediately	3.697	11.94	-1.811	1.177
Weakly	11.09	35.83	-1.811	1.177

Based on the response spectrum and coherency loss function, three-dimensional spatially varying ground motions at four supports of the example bridge are simulated independently. The intensity of the vertical component is assumed to be 0.67 times of the horizontal components whose peak ground acceleration (PGA) is 0.4g. The duration and time interval of the simulated time-histories are 20.47 and 0.01s, respectively. More detailed information about the spatially varying ground motion simulation can be found in Bi and Hao[39].

Table 4. Spatially varying ground motion cases

Case	v_{app} (m/s)	Coherency	Site
1	infinite	Perfectly	FFFF
2	500	Perfectly	FFFF
3	infinite	Intermediately	FFFF
4	500	Intermediately	FFFF
5	1000	Intermediately	FFFF
6	200	Intermediately	FFFF
7	500	Highly	FFFF
8	500	Weakly	FFFF
9	500	Intermediately	MFFM
10	500	Intermediately	MMMM

A total of 10 cases of spatially varying ground motions are simulated by considering different wave propagation apparent velocities (v_{app}), coherency loss and local site conditions, as shown in Table 4. For each case, 120 sets of spatially varying ground motion time histories are simulated, and each set consists of twelve time histories, i.e., two horizontal and one vertical spatial motion at each of the four supports. Case 1 represents uniform ground motions in which infinite wave propagation apparent velocity and no coherency loss are assumed. Case 2 and Case 3 correspond to spatially varying ground motions with wave passage effect only and with coherency loss effect only, respectively; Case 4 is a "benchmark case" which considers both wave passage effect (v_{app}=500m/s) and coherency loss effect (intermediately correlated), and the following cases are designed by changing the wave propagation apparent velocity, coherency loss or local site conditions with respect to Case 4. In Table 4, the "FFFF" and "MMMM" respectively represent homogeneous firm site and

homogeneous medium site, while "MFFM" represents the heterogeneous site with medium site beneath the abutment supports and firm site beneath the column supports.

Fig. 7 shows the horizontal in-plane spatial accelerations and displacements for the heterogeneous site (Case 9). It can be observed that the differences between the spatial motions at abutment supports and those at pier column supports are very evident because the local site effect further increases the spatial variations of the ground motions on the basis of wave passage and coherency loss effect. Figs. 8 and 9 show the response spectra and coherency losses of the simulated ground motions and the prescribed models, good matches can be observed. It should be noted that only horizontal in-plane motions are plotted in Figs. 7 to 9. The horizontal out-of-plane and vertical in-plane motions are not plotted for conciseness. Good agreements can be observed as well.

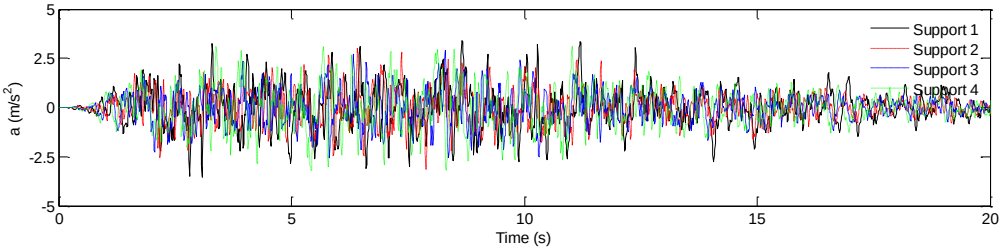

(a) Accelerations

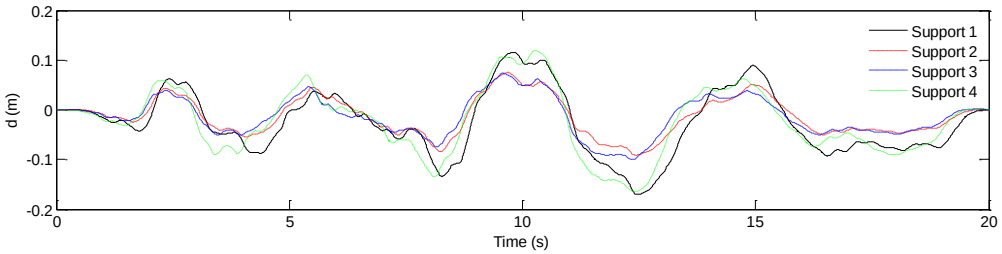

(b) Displacements

Fig. 7. Generated spatially varying ground motions on heterogeneous site (Case 9)

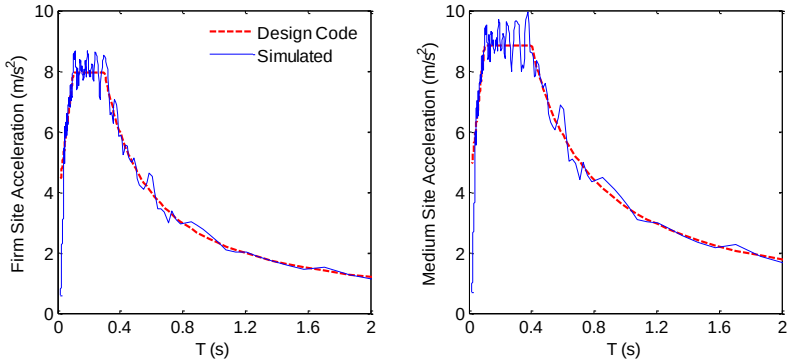

Fig. 8. Comparison of the simulated acceleration and the code response spectrum

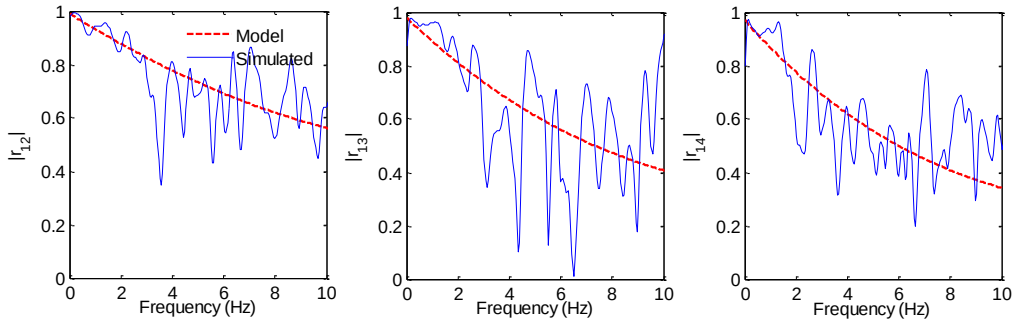

Fig. 9. Comparison of the coherency loss between simulated ground motions and the empirical function

4. Seismic Fragility Analysis Methodology

The seismic fragility analytical method based on the nonlinear time history analysis is employed to calculate the lifetime seismic fragility of the example RC bridge subjected to spatially varying ground motions. Fragility curves can be generated by using the incremental dynamic analysis (IDA) method or the probabilistic seismic demand analysis (PSDA) method.[41] Since a huge computational effort is required for the IDA method in which a huge amount of nonlinear time history analyses are conducted using scaled seismic ground motions, the PSDA method is adopted in this study.

PSDA method is developed by calculating the structural seismic response through time history analysis with a large number of earthquake ground motions which cover a wide range of an intensity measure, and then conducting regression analysis between the seismic demand data and the intensity measure. The relationship of median engineering demand parameter (EDP) and the selected intensity measure (IM) can be expressed with a powerful log-linear model suggested by Cornell *et al.*[42]:

$$\mathrm{EDP} = a(\mathrm{IM})^b \text{ or } \ln(\mathrm{EDP}) = \ln a + b\ln(\mathrm{IM}) \tag{12}$$

in which a and b are regression coefficients. By assuming that the EDP at a certain IM coincides with a log-normal probabilistic distribution, the conditional probability for a bridge to reach a damage limit state (LS) under a certain IM, namely the seismic fragility of the bridge, can be developed as[35]:

$$P[\mathrm{EDP} \geq LS \,|\, \mathrm{IM}] = \Phi\left(\frac{\ln(\mathrm{IM}) - \ln(\mu_{\mathrm{IM}})}{\sigma_{\mathrm{IM}}}\right) \tag{13}$$

where

$$\ln(\mu_{\mathrm{IM}}) = \frac{\ln(LS) - \ln(a)}{b} \text{ and } \sigma_{\mathrm{IM}} = \frac{\xi_{\mathrm{EDP|IM}}}{b} \tag{14}$$

in which $\Phi(\bullet)$ represents the standard normal distribution function, μ_{IM} and σ_{IM} are the mean value and standard deviation of IM in the fragility function. $\xi_{\mathrm{EDP|IM}}$ is the standard deviation derived from the log-linear regression analysis between EDP and IM, which can be represented as

$$\xi_{EDP|IM} = \sqrt{S_r/(n-2)} \tag{15}$$

where S_r is the residual sum of squares in the log-linear regression analysis, n is the number of the nonlinear time history analyses. Therefore, using the parameters obtained from log-linear regression analysis between EDP and IM, the analytical seismic fragility curves can be generated based on Eq. (13).

As suggested by previous studies[41, 43], good linear consistency between EDP and IM in the logarithmic coordinate system can be achieved when PGA is selected as the IM, indicating that it can be a good choice of IM. Therefore, PGA is selected as the IM to develop the seismic fragility analysis in the current paper. Since the simulated spatially varying ground motions are taken as inputs, the intensities of the ground motions at different supports are different. The maximum horizontal PGA of the ground motion at the left abutment (Support 1 in Fig. 2) is selected as the IM for each set of spatial ground motions in this study. Moreover, it is required by the PSDA method that the earthquake ground motions should cover a wide range of PGA; therefore, the simulated spatially varying acceleration time histories are scaled based on the maximum horizontal PGA of the ground motions at the left abutment. The 120 sets of spatially varying ground motions in each case are equally divided into 10 groups, among the 12 sets of ground motions in a certain group, the nth set is scaled to the target PGA which is valued stochastically between $(0.1n\text{-}0.1)$g and $(0.1n)$g. As a result, for each

ground motion case, the PGAs of the 120 sets of spatially varying time histories are stochastically distributed in the range of 0-1.2g with 10 sets in each interval of 0.1g.

Different levels of damage to different components of bridge structures may be induced by earthquake actions. It is of great significance to properly define a damage index that well describes the conditions of bridge structures. For the example RC rigid frame bridge, the damage state can be reasonably described by the damage of pier columns since they are the most vulnerable components, as well as the critical load-carrying members; therefore, the seismic fragility of the pier columns are utilized to represent the fragility of the whole bridge in this study. Moreover, the column curvature ductility, which is the ratio of the maximum column curvature obtained from the nonlinear time history analysis to the column yield curvature obtained from the Pushover analysis, is taken as the damage index of the example RC bridge. The four damage limit states defined by HAZUS[44], namely slight, moderate, extensive, and complete damage, and the corresponding column curvature ductility of 1, 2, 4 and 7 suggested by Choi *et al.*[3] are employed to generate the seismic fragility curves.

5. Results and Discussion

Nonlinear time history analyses are conducted for the example RC bridge models at different time steps under the spatially varying ground motions. The seismic fragility curves are generated by using the PSDA method based on Eq. (13). As stated above, a total of 10 bridge models are developed at each time step with a 15-year interval after the corrosion initiation time, the 10 bridge models are corresponded with 10 groups of spatially varying ground motion in every case. Response analyses of each of the 10 bridge models subjected to 12 sets of simulated spatial ground motions in one of the 10 ground motion groups are carried out. Therefore, a total number of 10 (cases) $\times$7 (time steps) $\times$10 (bridge models) $\times$12 (sets of ground motions) =8400 nonlinear time history analyses are carried out in the present study. Moreover, Pushover analysis is also conducted to calculate the yield curvature of the columns for every bridge model at every time step during the bridge's life-cycle.

Fig. 10 shows the calculated column curvature ductility with respect to ground motion PGA in the logarithm coordinate through a total of 120 nonlinear time history analyses for the intact bridge (t_i=0) and the corroded bridge (t_i=90 years) under uniform ground motions. Based on Eqs. (12) and (14), the constants of a, b and $\zeta_{EDP|IM}$ can be obtained through the linear regression analysis of the simulated data. The mean and standard deviation of PGA required to reach four damage limit states at different time steps under uniform ground motions (Case 1) are summarized in Table 5, and the corresponding seismic fragility curves are shown in Fig. 11.

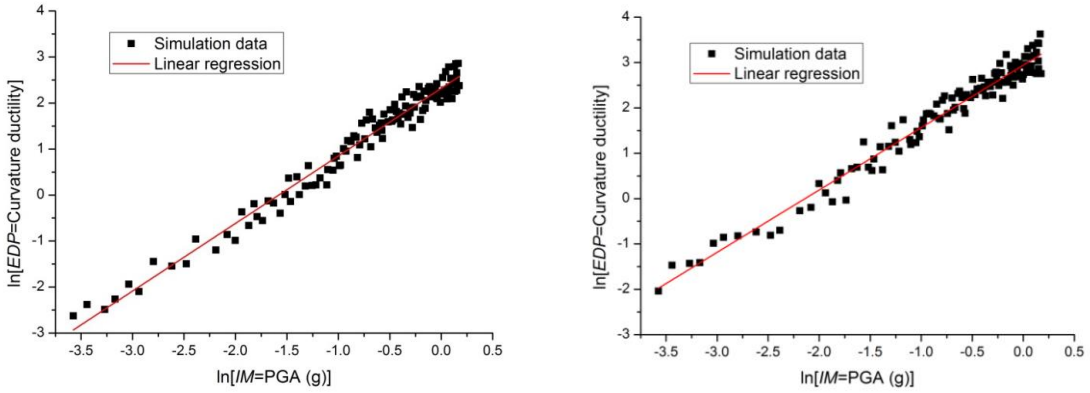

(a) t_i=0 (b) t_i=90 years

Fig. 10. Regression analysis of the column curvature ductility with respect to ground motion PGAs (Case 1)

As shown in Table 5, the mean PGAs that would cause bridge damage decrease with time owing to the chloride induced corrosion effect. After 90 years since corrosion initiation, the

mean PGA required to cause slight, moderate, extensive and complete damage of the bridge under consideration decreases by 42.7%, 41.1%, 39.1% and 37.5%, respectively. It should be noted that the standard deviations of PGA of the fragility curves derived from PSDA method are the same for all the four damage limit states[41] and no apparent variation with aging time is found. They are in the range of 0.15-0.20 as listed in Table 5. It can be seen from the seismic fragility curves that, as expected, the damage probability of the RC bridge increases with time. Moreover, the fragility curves corresponding to different years move closer to each other with time, i.e., the fragility curves corresponding to 75 and 90 years are closer to each other than those between 15 and 30 years. This is because the corrosion rate of the column reinforcements decreases as the corrosion current density decreases with time, resulting in a smaller deterioration rate of the bridge.

Table 5. Means and standard deviations of seismic fragility of the example bridge at different time steps (Case 1)

t_i (years)		0	15	30	45	60	75	90
μ_{IM} (g)	Slight	0.206	0.180	0.167	0.151	0.133	0.125	0.118
	Moderate	0.331	0.291	0.270	0.251	0.222	0.203	0.195
	Extensive	0.530	0.469	0.442	0.411	0.364	0.346	0.323
	Complete	0.776	0.689	0.657	0.598	0.563	0.505	0.485
σ_{IM}		0.151	0.162	0.165	0.164	0.156	0.168	0.165

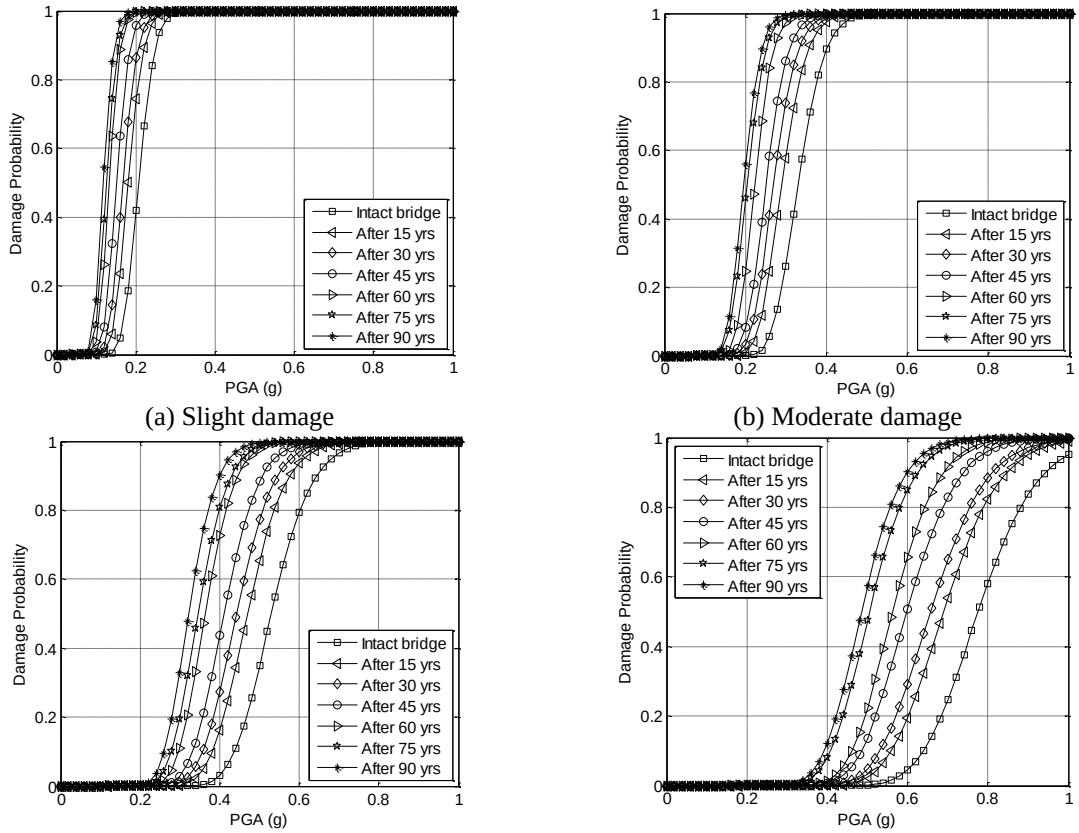

(a) Slight damage (b) Moderate damage

(c) Extensive damage (d) Complete damage

Fig. 11. Seismic fragility curves of the example bridge at different time steps (Case 1)

To further investigate the increasing trend of the seismic fragility of the chloride corroded RC bridge during its service life, the regression analysis is carried out to fit the relationship between the mean PGA required to cause certain damage and the time after corrosion initiation. It is found that the relationship between these two factors fits well with a quadratic polynomial, i.e.:

$$\mu_{PGA}(t_i) = k_0 + k_1 t_i + k_2 t_i^2 \tag{16}$$

where t_i is the time after corrosion initiation in years, $\mu_{PGA}(t_i)$ is the mean PGA for a bridge to reach different damage limit states, k_0, k_1, k_2 are regression coefficients.

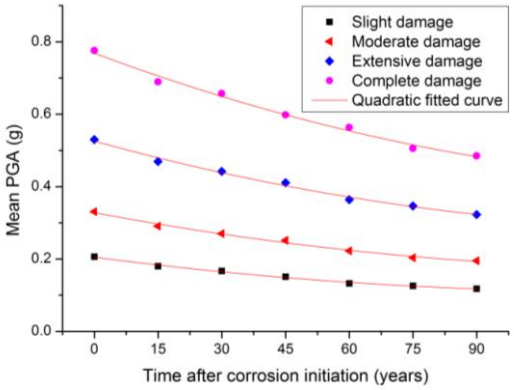

Fig. 12. Time-dependent mean PGAs and the corresponding fitted curves (Case 1)

Table 6. Coefficients of the regression analysis of $\mu_{PGA}(t_i)$ (Case 1)

Damage state	k_0	k_1	k_2	R^2
Slight	0.205	-0.0015	6.229×10^{-6}	0.991
Moderate	0.328	-0.0022	7.731×10^{-6}	0.989
Extensive	0.526	-0.0032	1.080×10^{-5}	0.988
Complete	0.768	-0.0044	1.323×10^{-5}	0.986

Fig. 12 shows the time-dependent mean PGAs for a bridge to suffer different level of damages and the corresponding quadratic fitted curves, the regression coefficients are listed in Table 6. It can be seen that very good agreements are achieved. As shown, the mean PGAs required to cause bridge damage decreases, but the decreasing rate slows down with time. This is caused by the decrease of the corrosion current density in the bridge's service life as discussed above. The best fitted functions can be used to estimate the mean PGA that would induce certain level of damage to the bridge model considered in this study for a number of years after corrosion initiation time.

The simulation results indicate that the seismic fragility show nearly the same degradation trend for all the four damage limit states. Therefore, for conciseness, only the results corresponding to the extensive damage is presented and discussed in detail hereafter.

5.1. Effects of ground motion spatial variations

To examine the effects of ground motion spatial variations on the seismic fragility of the corroded RC bridge, the seismic fragility curves corresponding to the ground motion Cases 1-4 are generated. Fig. 13 shows the seismic fragility curves (t_i=0 and 90 years) and time-dependent mean PGAs for the extensive damage limit state under the four ground motion cases, and the regression coefficients of the fitted curves are given in Table 7. As shown, the seismic fragility of the RC bridge increases with time for all the ground motion cases. Completely neglecting ground motion spatial variation, i.e., the uniform ground motion case (Case 1), over predicts the seismic fragilities of the bridge as compared with those corresponding to the general case (Case 4). Considering only coherency loss effect (Case 3) results in the largest fragility, while considering only wave passage effect (Case 2) always underestimates the fragility. The seismic fragilities under the spatially varying ground motion cases with wave passage effect (Cases 2 and 4) are lower than those of the cases without wave passage effect (Cases 1 and 3). For the cases with the same wave passage effect, the seismic fragilities of the spatial ground motion case with coherency loss effect (Cases 3 and 4) are higher than those of the cases without coherency loss effect (Cases 1 and 2).

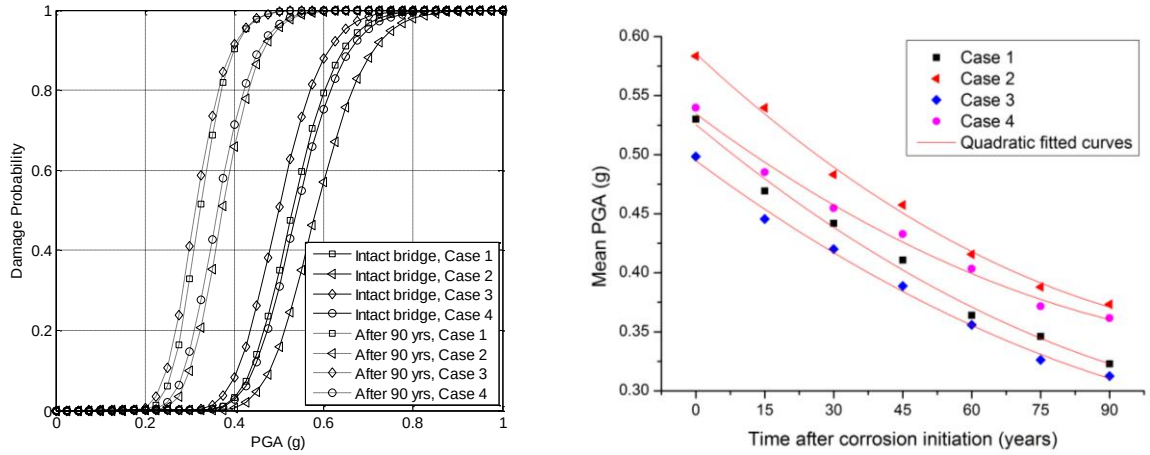

Fig. 13. Seismic fragility curves (t_i=0 and t_i=90 years) and time-dependent mean PGAs under ground motions Cases 1-4

Table 7. Regression coefficients of $\mu_{PGA}(t_i)$ for ground motion Cases 1-4

Case	k_0	k_1	k_2	R^2
1	0.526	-0.0032	1.080×10^{-5}	0.988
2	0.586	-0.0036	1.362×10^{-5}	0.994
3	0.495	-0.0029	9.116×10^{-6}	0.992
4	0.535	-0.0029	1.064×10^{-5}	0.987

Moreover, compared with the intact bridge (t_i=0), the mean PGA required to generate extensive damage to the corroded bridge (t_i=90 years) decreases by 39.1%, 36.0%, 37.3% and 33.0% for Case 1 to Case 4, respectively. The mean PGAs for different cases show a slightly different attenuation rate with time, implying the dominant ground motion spatial variation effect on bridge responses changes with time. The difference of mean PGAs between the cases with different coherency loss (Cases 1 and 3; Cases 2 and 4) becomes smaller with time, and the cases with the same wave passage effect have rather similar seismic fragilities for the corroded bridge after being in service for 90 years since corrosion initiated. These results imply that the seismic fragilities of the corroded bridge are more affected by spatial ground motion wave passage effect. This is because that the chloride corrosion damage leads to bridge stiffness deterioration, and spatial ground motion wave passage effect is more pronounced to relatively flexible structures, while coherency loss effect is more prominent to relatively stiff structures, as reported by Hao and Duan[45].

The above analysis highlighted the importance of ground motion spatial variations on the seismic fragility of RC bridges subjected to chloride corrosion. Neglecting ground motion spatial variations may lead to an inaccurate estimation on the seismic fragility of the corroded RC bridge during its life-cycle.

5.2. Wave passage effect

Previous studies[46] revealed that the ground motion wave propagation apparent velocity is very irregular and frequency dependent, therefore there is no generally applicable model yet to represent it. In the spatially varying ground motion simulations, it is generally assumed as a constant. Four apparent velocities, namely infinite (Case 3), 1000m/s (Case 5), 500m/s(Case 4) and 200m/s (Case 6) are assumed in this study to analyse the wave passage effect on the seismic fragility of the RC bridge. Intermediately coherency loss and homogeneous firm site condition are assumed for all these four cases, so that the apparent wave velocity is the only varying parameter among them.

Fig. 14 shows the seismic fragility curves (t_i=0 and 90 years) and the time-dependent mean PGAs corresponding to the extensive damage limit state under spatial ground motion cases with different apparent wave velocities, and the coefficients of the regression analyses are

listed in Table 8. It is shown that the seismic fragilities under the case of infinite apparent wave velocity (Case 3) are always the largest for the corroded bridges at different time steps, and the fragility decreases as the apparent wave velocity decreases. These results again indicate that spatial ground motion wave passage effect reduces the responses and damage probability of the bridge under consideration. Relative to the intact bridge, the mean PGAs of fragility for the corroded RC bridge (t_i=90 years) decrease by 37.3%, 33.9%, 33.0% and 29.9% for Cases 3, 5, 4 and 6, respectively. The difference between the mean PGAs among the four spatial ground motion cases increase with time during the bridge's life-cycle. Table 9 summarizes the differences in percentage of the mean PGAs under ground motion cases with different apparent wave velocities at every time step. The difference in percentage is defined as the ratio of the maximum difference value to the average value of the mean PGAs under four cases at a certain time step, and it is calculated by using both the data from original simulation results (Original difference) and regression analysis results (Regression difference) in this study. The increase of difference of mean PGAs leads the fragility curves of the corroded bridge under four spatial ground motion cases to separate from each other as compared to those of the intact bridge. These results indicate that the wave passage effect becomes relatively more significant on the responses and hence the seismic fragility of the corroded RC bridge because it is comparatively more flexible as discussed above.

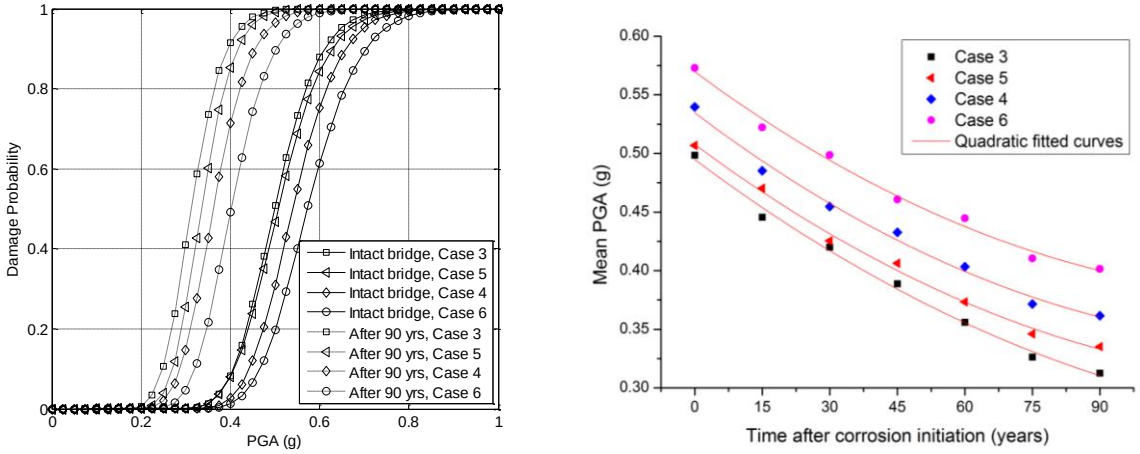

Fig. 14. Seismic fragility curves (t_i=0 and t_i=90 years) and time-dependent mean PGAs under spatial ground motion cases with different apparent wave velocities

Table 8. Regression coefficients of $\mu_{PGA}(t_i)$ for spatial ground motion cases with different apparent wave velocities

Case	k_0	k_1	k_2	R^2
3	0.495	-0.0029	9.116×10^{-6}	0.992
5	0.508	-0.0028	1.001×10^{-5}	0.993
4	0.535	-0.0029	1.064×10^{-5}	0.987
6	0.570	-0.0028	1.053×10^{-5}	0.988

Table 9. The difference in percentage of the mean PGAs under spatial ground motion cases with different apparent wave velocities at different time steps

t_i (years)	0	15	30	45	60	75	90
Original difference	14.08%	15.94%	17.50%	17.09%	22.54%	23.19%	25.24%
Regression difference	14.20%	15.57%	17.18%	18.99%	21.02%	23.25%	25.60%

The above results demonstrate that neglecting the ground motion wave passage effect may lead to a significant error in the fragility estimation for the corroded RC bridges, and the effect of wave passage effect on the seismic fragility increases with the proceeding of chloride induced corrosion. Therefore, it is essential to consider the wave passage effect in the seismic fragility analysis of the corroded RC bridges.

5.3. Coherency loss effect

To investigate the spatial ground motion coherency loss effect on the seismic fragility of corroded RC bridges, four spatial ground motion cases with different coherency losses, namely perfectly correlated (Case 2), highly correlated (Case 7), intermediately correlated (Case 4) and weakly correlated (Case 8) are considered. The apparent wave velocity of 500m/s and the homogeneous firm site condition are assumed for all these cases to ensure that the only difference among them is the coherency loss.

Fig. 15 shows the seismic fragility curves (t_i=0 and 90 years) and the time-dependent mean PGAs corresponding to the extensive damage under spatial ground motion cases with different coherency losses, and the coefficients of regression analyses are summarized in Table 10. As shown, the seismic fragilities under the weakly correlated spatial ground motions (Case 8) are always the largest for the corroded bridges at different time steps, and the fragility increases with the increase of spatial ground motion coherency loss, indicating that the less correlated spatial ground motions are more damaging to the bridge. Relative to the intact bridge, the mean PGAs of fragility for the corroded RC bridge (t_i=90 years) decrease by 36.0%, 35.2%, 33.0% and 28.1% for Cases 2, 7, 4 and 8, respectively. The difference in the mean PGAs for the four cases decreases with time during the bridge's life-cycle as summarized in Table 11. The decrease of difference of mean PGAs leads the fragility curves under ground motion cases with different coherency losses to become relatively closer with each other; These results indicate that the coherency loss effect becomes relatively less significant on the seismic fragility of the progressively corroded RC bridge owning to the continuously deteriorating bridge stiffness.

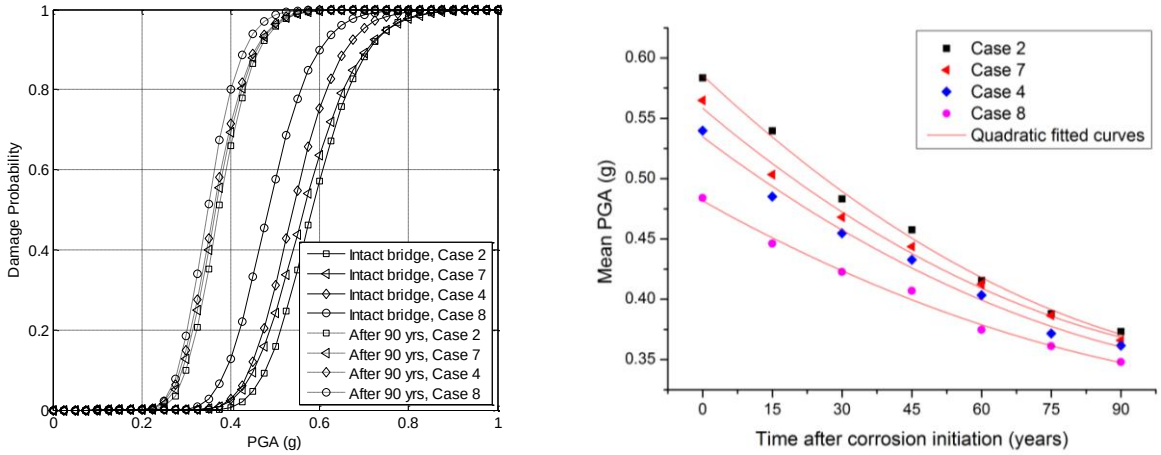

Fig. 15. Seismic fragility curves (t_i=0 and t_i=90 years) and time-dependent mean PGAs under spatial ground motion cases with different coherency losses

Table 10. Regression coefficients of $\mu_{PGA}(t_i)$ for spatial ground motions with different coherency losses

Case	k_0	k_1	k_2	R^2
2	0.586	-0.0036	1.362×10^{-5}	0.994
7	0.558	-0.0032	1.258×10^{-5}	0.990
4	0.535	-0.0029	1.064×10^{-5}	0.987
8	0.482	-0.0022	7.404×10^{-6}	0.989

Table 11. The difference in percentage of the mean PGAs under spatial ground motions with different coherency losses at different time steps

t_i (years)	0	15	30	45	60	75	90
Sample difference	18.33%	18.94%	13.27%	11.61%	10.19%	7.09%	6.99%
Regression difference	19.26%	16.79%	14.35%	11.99%	9.82%	7.97%	6.58%

The above analyses illustrate the significance of spatial ground motion coherency loss effect on the seismic fragility of RC bridges. Although the influence of the coherency loss

effect may decrease with the proceeding of chloride induced corrosion, neglecting the spatial coherency loss may lead to an inaccurate prediction of the seismic fragility of the chloride corroded RC bridges during its life-cycle.

5.4. Local site effect

Three local site conditions are considered in this study to investigate the spatial ground motion local site effect on the seismic fragility of the corroded RC bridge. These cases include homogeneous firm site (Case 4), heterogeneous site with firm soil on the column supports and medium soil on the abutment supports (Case 9) and homogeneous medium site (Case 10). The same apparent wave velocity (500 m/s) and coherency loss (intermediately correlated) are assumed for the three spatial ground motion cases; therefore the local site effect is the only difference between them.

Fig. 16 shows the seismic fragility curves (t_i=0 and 90 years) and the time-dependent mean PGAs for the extensive damage limit state under spatial ground motions with different site conditions, and the coefficients of the regression analyses of $\mu_{PGA}(t_i)$ are given in Table 12. It is shown that the seismic fragilities under the spatial ground motion case with heterogeneous site condition (Case 9) are always the largest for the corroded bridge at different time steps, followed by the homogeneous medium site (Case 10) and the homogeneous firm site (Case 4), indicating the local site conditions have a great effect on the seismic fragility of the bridge structure. As shown the seismic fragility of the intact bridge under the heterogeneous site condition (Case 9) is even larger than that of the corroded bridge (t_i=90 years) under the homogeneous firm site condition (Case 4), implying the influences of the heterogeneous site conditions on bridge damage probability could be more significant than the 90-years chloride induced corrosion damage. Relative to the intact bridge, the mean PGAs of fragility for the corroded RC bridge (t_i=90 years) decrease by 33.0%, 35.5% and 37.3% for Cases 4, 9 and 10, respectively. It is shown that the degradation rates of the mean PGAs for the three spatial ground motion cases are basically the same in the bridge's life-cycle. The differences in percentage of the mean PGAs corresponding to the three spatial ground motion cases are given in Table 13. It can be seen that the differences in percentage vary between 43.5% and 50.1%, and there is no obvious trend with time. These results indicate that the effect of ground motion spatial variation induced by changing site conditions does not change with bridge conditions, which is different from the spatial ground motion wave passage and coherency loss effects as observed above.

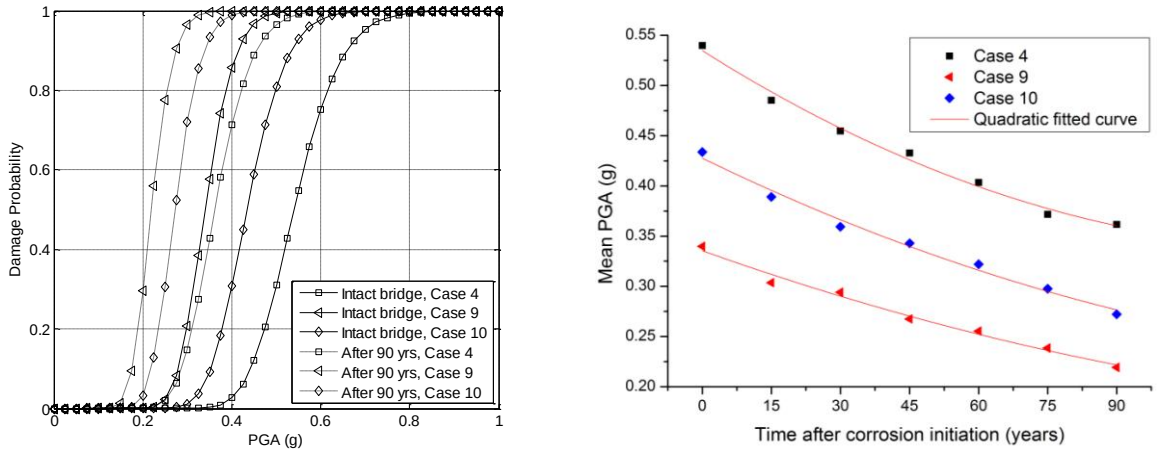

Fig. 16. Seismic fragility curves (t_i=0 and t_i=90 years) and time-dependent mean PGAs under spatial ground motion cases with different local site conditions

Table 12. Coefficients of the regression analysis of $\mu_{PGA}(t_i)$ for spatial ground motions with different local site conditions

Case	k_0	k_1	k_2	R^2

4	0.535	-0.0029	1.064×10^{-5}	0.987
9	0.335	-0.0016	4.068×10^{-6}	0.981
10	0.428	-0.0022	6.070×10^{-6}	0.983

Table 13. The difference in percentage of the mean PGAs under spatial ground motions with different local site conditions at different time steps

t_i (years)	0	15	30	45	60	75	90
Sample difference	45.68%	46.26%	43.51%	47.54%	45.25%	43.97%	50.05%
Regression difference	46.07%	45.40%	45.05%	45.12%	45.68%	46.79%	48.55%

The above results demonstrated that the ground motion spatial variations induced by changing local site conditions have a significant influence on bridge seismic fragility. Neglecting the local site effect on modelling the ground motion spatial variations may lead to a substantial underestimation of the seismic fragility of the corroded RC bridge during its service life.

6. Conclusions

This paper investigates the seismic fragility of a RC bridge with chloride induced corrosion subjected to spatial ground motions. Based on the analytical results, the following conclusions can be drawn:

1. Both the chloride induced corrosion and ground motion spatial variations can have a significant effect on the lifetime seismic fragility of the RC bridge. To achieve more realistically estimated seismic fragilities of RC bridges, neither of these two factors should be neglected.
2. The seismic fragility increases during the bridge's life-cycle due to the chloride induced corrosion effect. The mean PGAs of corresponding fragility curves decrease and the attenuation rates slow down with time owing to the decrease of corrosion rate of the reinforcements.
3. Both the spatial ground motion wave passage effect and coherency loss effect have significant influences on bridge structural responses and hence on the seismic fragility. Along with the proceeding of chloride induced corrosion, owing to the reduction of the structural stiffness, the spatial ground motion wave passage effect becomes more pronounced, while the spatial ground motion coherency loss effect becomes less prominent. It should be noted that the corrosion damage of superstructure, which is not considered in this paper, can further contribute to the reduction of the structural stiffness. The changing of the effect of spatial ground motion wave passage and coherency loss would therefore be expected more prominent on the seismic fragility of the RC bridge during its life-cycle.
4. The ground motion spatial variation induced by varying local site conditions is very significant on the bridge seismic fragility. Neglecting the heterogeneous site condition across the bridge supports may greatly underestimate the seismic fragilities of RC bridges.

It should be noted that the conclusions drawn in this paper are based on the example continuous rigid frame RC bridge, which is a common type in the highway bridges; for the lifetime seismic fragility analyses of other types of bridge structures subjected to spatially varying ground motions, further studies should be carried out in the future. Nonetheless, the seismic fragility analysis method in this study can provide references for more reasonable seismic damage cost estimation, life-cycle cost analysis, as well as maintenance strategies of RC bridges exposed to chloride corrosion damage.

Acknowledgements

The authors would like to acknowledge the financial support from the National Basic Research Program of China (973 program, Grant No. 2011CB013605) to carry out this research. The first author would like to thank the China Scholarship Council for providing financial support for him to study in Curtin University as a visiting PhD student.

References

1. Mander, J.B. and Basoz, N. Seismic fragility curve theory for highway bridges, *Proceedings of 5th US Conference on Lifeline Earthquake Engineering*, Seattle, USA (1999).
2. Hwang, H., Liu, J. and Chiu, Y. Seismic fragility analysis of highway bridges, *MAEC RR-4*, Center for Earthquake Research Information (2001).
3. Choi, E., DesRoches, R. and Nielson, B. Seismic fragility of typical bridges in moderate seismic zones, *Eng. Struct.* **26**(2) (2004) 187-199.
4. Lin, J. H. Seismic fragility analysis of frame structures, *Int. J. Struct. Stab. Dyn.* **8**(3) (2008) 451-463.
5. Basoz, N., Kiremidjian, A.S., King, S.A. and Law, K.H. Statistical analysis of bridge damage data from the 1994 Northridge, CA, earthquake, *Earthq. Spectra.* **15**(1) (1999) 25-54.
6. Shinozuka, M., Feng, M.Q., Lee, J. and Naganuma, T. Statistical analysis of fragility curves, *J. Eng. Mech.* **126**(12) (2000) 1224-1231.
7. Karim, K.R. and Yamazaki, F. A simplified method of constructing fragility curves for highway bridges, *Earthq. Eng. Struc. Dyn.* **32**(10) (2003) 1603-1626.
8. Mackie, K.R. and Stojadinovic, B. Fragility curves for reinforced concrete highway overpass bridges, *Proceedings of 13th World Conference on Earthquake Engineering*, Vancouver, BC, Canada (2004).
9. Nielson, B.G. and Desroches, R. Seismic fragility methodology for highway bridges using a component level approach, *Earthq. Eng. Struc. Dyn.* **36**(6) (2007) 823-839.
10. Abdel-Mohti, A. and Pekcan, G. Effect of skew angle on seismic vulnerability of RC box-girder highway bridges. *Int. J. Struc. Stab. Dyn*. **13**(06) (2013) 1-24.
11. ASCE. Report card for America's infrastructure (2013) (http://www.infrastructurereportcard.org/a/browser-options/ downloads/2013-Report-Card.pdf).
12. Enright, M.P. and Frangopol, D.M. Probabilistic analysis of resistance degradation of reinforced concrete bridge beams under corrosion, *Eng. Struct.* **20**(11) (1998) 960-971.
13. Stewart, M.G. and Rosowsky, D.V. Time-dependent reliability of deteriorating reinforced concrete bridge decks, *Struct. Saf.* **20**(1) (1998) 91-109.
14. Choe, D.E., Gardoni, P., Rosowsky, D. and Haukaas, T. Seismic fragility estimates for reinforced concrete bridges subject to corrosion, *Struct. Saf.* **31**(4) (2009) 275-283.
15. Simon, J., Bracci, J.M. and Gardoni, P. Seismic response and fragility of deteriorated reinforced concrete bridges, *J. Struct. Eng*. **136**(10) (2010) 1273-1281.
16. Alipour, A., Shafei, B. and Shinozuka, M. Performance evaluation of deteriorating highway bridges located in high seismic areas, *J. Bridge Eng.***16**(5) (2010) 597-611.
17. Ghosh, J. and Padgett, J.E. Aging considerations in the development of time-dependent seismic fragility curves, *J. Struct. Eng*. **136**(12) (2010) 1497-1511.
18. Yalcyn, H. and Ergun, M. The prediction of corrosion rates of reinforcing steels in concrete, *Cement Concrete Res.* **26**(10) (1996) 1593-1599.
19. Liu, T. and Weyers, R.W. Modeling the dynamic corrosion process in chloride contaminated concrete structures, *Cement Concrete Res.* **28**(3) (1998) 365-379.
20. Vu, K.A.T. and Stewart, M.G. Structural reliability of concrete bridges including improved chloride-induced corrosion models, *Struct. Saf.* **22**(4) (2000) 313-333.
21. Hao, H. Arch responses to correlated multiple excitations, *Earthq. Eng. Struct. Dyn.* **22**(5) (1993) 389-404.
22. Zanardo, G., Hao, H. and Modena, C. Seismic response of multi-span simply supported bridges to spatially varying earthquake ground motion, *Earthq. Eng. Struct. Dyn.* **31**(6) (2002) 1325-1345.
23. Soyluk, K., and Sicacik, E. A. Soil-structure interaction analysis of cable-stayed bridges for spatially varying ground motion components, *Soil Dyn. Earthq. Eng.* **35** (2012) 80-90.
24. Bi, K, Hao, H. and Chouw, N. 3D FEM analysis of pounding response of bridge structures at a canyon site to spatially varying ground motions, *Adv. Struct. Eng.* **16**(4) (2013) 619-640.
25. Deodatis, G., Saxena, V. and Shinozuka, M. Effect of spatial variability of ground motion on bridge fragility curves, *Proceedings of the 8th ASCE Specialty Conference on Probabilistic Mechanics and Structural Reliability*, University of Notre Dame, India (2000).
26. Kim, S.H. and Feng, M.Q. Fragility analysis of bridges under ground motion with spatial variation, *Int. J. Non-Linear Mech*. **38**(5) (2003) 705-721.
27. Lupoi, A., Franchin, P., Pinto, P.E. and Monti, G. Seismic design of bridges accounting for spatial variability of ground motion, *Earthq. Eng. Struct. Dyn*, **34**(4-5) (2005) 327-348.

28. Chouw, N. and Hao, H. Study of SSI and non-uniform ground motion effects on pounding between bridge girders, *Soil Dyn. Earthq. Eng*. **25**(7) (2005) 717-728.
29. JTG/T B02-01. Guidelines for Seismic Design of Highway Bridges, *Ministry of Communications of the People's Republic of China* (2008). (in Chinese)
30. McGee, R. Modelling of durability performance of Tasmanian bridges, *Proceedings of 8th International Conference on applications of statistics and probability in civil engineering*, Sydney, Australia (1999).
31. Hoffman, P.C. and Weyers, R.E. Probabilistic durability analysis of reinforced concrete bridge decks, *Probabilistic mechanics and structural reliability*, New York, USA (1996).
32. Du, Y.G., Clark, L.A. and Chan, A.H.C. "Residual capacity of corroded reinforcing bars", *Mag. Concrete Res.* **57**(3) (2005) 135-147.
33. Saifullah, M. (1994). "Effect of reinforcement corrosion on bond strength in reinforced concrete", *Ph.D. thesis*, The University of Birmingham, UK.
34. Kong, J.S., Ababneh, A.N., Frangopol, D.M. and Xi, Y. Reliability analysis of chloride penetration in saturated concrete, *Probab. Eng. Mech*. **17**(3) (2002) 305-315.
35. Nielson, B.G. Analytical fragility curves for highway bridges in moderate seismic zones, *Ph.D. thesis*, Georgia Institute of Technology, USA (2005).
36. Fang, C., Lundgren, K., Chen, L. and Zhu, C. Corrosion influence on bond in reinforced concrete, *Cement Concrete Res.* **34**(11) (2004) 2159-2167.
37. Mazzoni, S., McKenna, F., Scott, M.H., Fenves, G.L. and Jeremic, B. OpenSEES Command Language Manual, *PEER*, University of California Berkeley (2003).
38. Aviram, A., Mackie, K.R. and Stojadinovic, B. Guidelines for nonlinear analysis of bridge structures in California, *PEER Report 2008/03*, University of California Berkeley (2008).
39. Bi, K. and Hao, H. Modelling and simulation of spatially varying earthquake ground motions at sites with varying conditions, *Probab Eng. Mech*, **29** (2012) 92-104.
40. Hao, H., Oliveira, C.S. and Penzien, J. Multiple-station ground motion processing and simulation based on SMART-1 array data, *Nuclear Eng. Design*, **111**(3) (1989) 293-310.
41. Zhang, J. and Huo, Y. Evaluating effectiveness and optimum design of isolation devices for highway bridges using the fragility function method, *Eng. Struct*. **31**(8) (2009) 1648-1660.
42. Cornell, C.A., Jalayer, F., Hamburger, R.O. and Foutch, D.A. The probabilistic basis for the 2000 SAC/FEMA steel moment frame guidelines, *J. Struct. Eng*. **128**(4) (2002) 526-533.
43. Mackie, K.R. and Stojadinovic, B. Fragility basis for California highway overpass bridge seismic decision making, *PEER Report 2005/02*, University of California Berkeley (2005).
44. HAZUS. Earthquake loss estimation methodology, *National Institute of Building for the Federal Emergency Management Agency*, Washington D.C., USA (1997).
45. Hao, H. and Duan, X. Multiple excitation effects on response of symmetric building, *Eng. Struct.* **18**(9) (1996) 732-740.
46. Hao H. Effects of spatial variation of ground motions on large multiply-supported structures. *UCB/EERC-89-06*. University of California Berkeley (1989).